Proc. of the 9th Intl. Conf. of Asian Society for Precision Engg. and Nanotechnology (ASPEN 2022)
15–18 November 2022, Singapore. Edited by Nai Mui Ling Sharon and A. Senthil Kumar
doi://10.3850/978-981-18-6021-8_OR-01-0129

Powder reusability of Ti-48Al-2Cr-2Nb intermetallic in electron beam powder bed fusion process

Pan Wang[1, #], Wai Jack Sin[1], Mui Ling Sharon Nai[1], Fern Lan Ng[1], Aloysius Tan[1], Min Hao Goh[1] and Yusaku Maruno[2]

[1]Singapore Institute of Manufacturing Technology, 73 Nanyang Drive, 637662, Singapore

[2]Materials Solution Centre, Hitachi Metals Singapore Pte. Ltd., Singapore 629656

[#]Corresponding authors/Email: wangp@simtech.a-star.edu.sg, TEL:+65-67938957

KEYWORDS: Reuse times, TiAl intermetallic, Contaminations, Electron beam melting, Additive manufacturing

Metal powder bed fusion additive manufacturing (PBF-AM) has been widely adopted in the aerospace and orthopedic industries. For the powder feedstock used in PBF-AM, the condition of the metal powders affects the quality of the printed parts and the cost of the powder contributes to a significant portion of the overall manufacturing cost. It is not feasible to adopt virgin powder for every single build, therefore, the reuse of the powder feedstock in the subsequent builds becomes an economical method to reduce the cost. However, there is lack of standard methodology for the reusability of powder. In particular, the powder's quality may change with the increase of reuse times, which in turn causes the change of the PBF-AM part's quality. Herein, we evaluate the reusability of Ti-48Al-2Cr-2Nb intermetallic powder in the electron beam powder bed fusion (EB-PBF) process up to 15 times (totally ~ 300 h cumulative build time). The powders' characteristics, chemical compositions, microstructure, and mechanical properties of the EB-PBF parts are investigated to understand the mechanisms attributing to the change in powder quality. It is found that Ti-48Al-2Cr-2Nb powder can be reused up to 15 times without compromising the resultant microstructure and mechanical properties, even though the contaminations are unavoidable. These findings provide an in-depth understanding of the powder-process-microstructure relationship in additively manufactured Ti-48Al-2Cr-2Nb intermetallic samples and can be applied to other alloys with high volatile elemental content (e.g. Al, Mg, Zn, Pb, Mn).

1. Introduction

Metal powder bed fusion additive manufacturing (PBF-AM) has been widely adopted in many industry fields, such as aerospace, automotive and orthopedic industries [1, 2]. For a successful and repeatable PBF-AM process, metal powders conform to strict chemical and physical properties requirements. However, numerous factors affect characteristics of both virgin and reused powders.

Electron beam powder bed fusion (EB-PBF) is a representative PBF-AM technology for metals and alloys. Its high vacuum working environment makes it very suitable to process reactive materials [2]. In addition, the layer-by-layer preheating function using a defocused beam makes it ideal for materials that are prone to crack and/or have high brittle-to-ductile transition temperatures. Therefore, research on materials development [3, 4], process optimization [4-6], feasibility prototype [3, 7], and even production testing [8] are blowout in the past few years. With the technology and materials maturing to a higher technology readiness level, the qualification of the final component becomes more urgent, in which quality management of powder, as a feedstock, becomes more critical [9]. However, it is still not reported in the literature yet. Herein, we carried out a systemic study to understand the powder quality and the resultant parts property with reuse cycles up to 15 times using a popular aerospace grade Ti-48Al-2Cr-2Nb intermetallic and EB-PBF process.

2. Experimental procedures

The printing process was conducted with an Arcam A2X system with constant parameters set. The builds were defined from B1 for the first build performed with 50 kg of virgin powder and subsequently up to B15 for the final build. No new powder was added to the original 50 kg of powder after B1. While for the reused powder, R1 is defined as the 1st reused powder, while the R15 is the sieved powder after B15. The powder from the PRS process was then mixed with the unused powder remaining in the hoppers. After taking 340 g powder and sealing it into a clean dark glass container, all the rest of the powder was then filled to the hoppers for the subsequent build job.

The powder morphology and contaminants were characterized using Zeiss Ultra Plus field emission scanning electron microscope (SEM) coupled with energy dispersive X-ray spectroscopy (EDS) . The relevant particle characteristics were analyzed systemically [9]. Elemental depth profiling of virgin and reused Ti-48Al-2Cr-2Nb powders was performed using X-ray photoelectron spectroscopy (XPS). Sublimation or evaporation pressures of metallic elements and corresponding oxides at equilibrium were calculated with FactSage 8.1 [10] using FACT pure substances database, where the phases including all gaseous species, liquids, and solids were considered. In addition, the equilibrium oxygen partial pressure with respect to temperature was predicted for oxides.

Detailed characterization of microstructure and mechanical properties was carried out on the selected samples using SEM equipped with EDS and electron backscattered diffraction (EBSD). The X-ray diffraction (XRD, Bruker AXS D8 Advance X-ray diffractometer) operated at 40 kV and 40 mA was performed for structural analysis. Cylinder compression specimens with a diameter of 6 mm and a total height of 18 mm were cut from the rectangular sample. An Instron 5982 universal tensile testing machine with a 100 kN load cell and a video extensometer was used for the compressive testing with an initial strain rate of 3.3×10^{-4} s^{-1} at room temperature. At least three specimens were tested to calculate the average yield strength (YS) and compressive strain.

3. Results

Fig. 1 (a and b) show that the particle size distribution is within the required range of 45-150 μm in all the tested cycles. As the powder was being reused, the distribution curve became narrower due to the fusion of fine particles and their coalescence during the melting process, and larger agglomerated particles were being sieved out during the sieving process [11]. There was also a slight shift of the distribution curve to the right towards the larger particle size region. The narrowing of the distribution curve will lead to better powder flowability, as observed in the hall flow analysis. The D10 and D50 values increased slightly during the first two cycles compared to the virgin powder. After the first three cycles, D10 values kept almost the same, while D50 values reduced a bit after the first three cycles. On the other hand, the D90 value showed a continuous reduction as the powder was being reused. This is most likely due to the reused EB-PBF powders having been treated by blasting to break the bonds between particles during the powder recovery process [12].

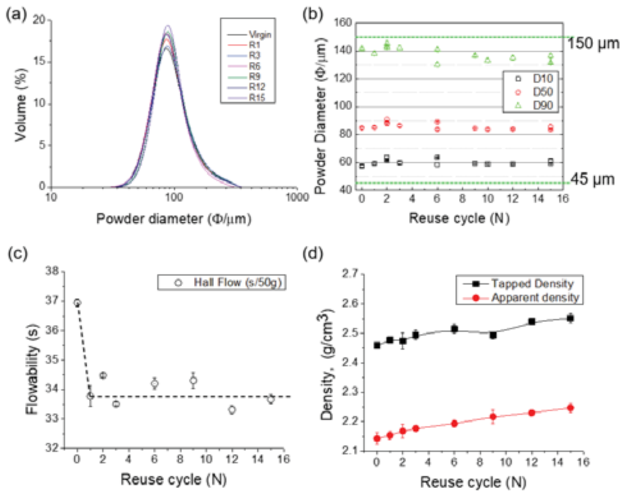

Fig. 1. Ti-48Al-2Cr-2Nb powder characteristics change with the increase of reuse cycle. (a) particle size distribution, (b) D10, D50 and D90, (c) flowability, (d) apparent density and tapped density.

Reused powders had better flowability as compared to virgin powder, as shown in Fig. 1 (c). After the first cycle, the flowability was comparable from cycles 1 to 15, although the fluctuation existed. The improvement in flowability could be due to moisture within the powders being removed as the Ti-48Al-2Cr-2Nb powders are being held at elevated temperatures and in a vacuum during the EB-PBF process [13]. Fig. 1 (d) show a slight increase in apparent density and tapped density as the powders undergo more reuse cycles. Relative apparent density increased from 52.7% to 55.4%, while relative tapped density raised from 60.6% to 62.8%. It is to be noted that the true density of the powder measured using Helium pycnometer was 4.06 g/cm^3. The increase in both apparent and tapped density indicates a better packing density of the deposited powders in layers [13]. The powder morphology and particle size distribution could also play a part in the apparent density of the powder [12].

A detailed inspection shows that the virgin powder had a few satellites attached to the particle surfaces and the entrapped gas pores, as depicted in Fig. 2(a). This is a common phenomenon for the gas atomized powder [9]. It also should be mentioned that the grains and boundaries were clearly visible at higher magnification, and the particle surfaces were immaculate (Fig. 2a′). After the 1st reuse cycle (Fig. 2b), the number of satellites reduced significantly (Fig. 2a and b). This may associate with the change in flowability (Fig. 1c). The grains and boundaries were still visible from a zoomed-in observation, although deformed surface and remnants were observed (Fig. 2b′ and b″). In addition, melt the covered surface of the particle was also observed (Fig. 2b‴). The presence of melt-covered particles is due to the spattering of the powder bed during the melting process and the melted residues were falling onto nearby particles. After the 2nd reuse cycle (Fig. 2c), a damaged surface and a crack from the connection between a satellite and the powder were observed. The damaged surface could be due to blasting and breaking up the pre-sintered large powder clumps and the satellited powder by compressed air at high pressure during the powder recovery process in the PRS, while the crack indicated the breaking of the bond between the powder and its satellites.

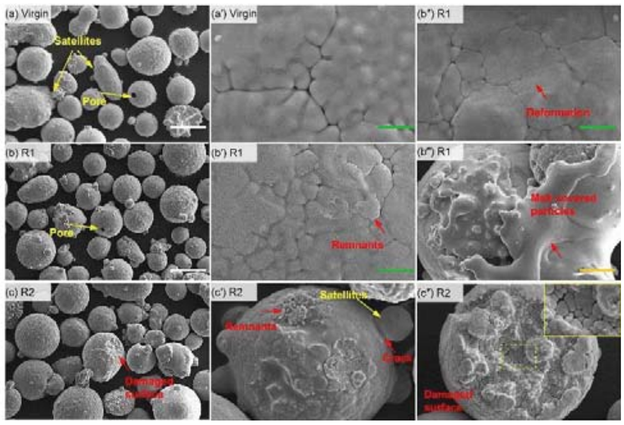

Fig. 2. SEM images of (a) virgin, (b) R1, (c) R2, and (d) R3 Ti-48Al-2Cr-2Nb powders at varied magnifications. (White scale bar = 100 μm, orange scale bar = 20 μm, and green scale bar = 4 μm).

Fig. 3 (a) depicts the chemical composition changes for four main elements, Ti, Al, Cr, and Nb, by EDS among the 15 reuse cycles. EDS results show a gradual decrease in Al content and increased Ti content with increasing reuse cycles. This may occur due to the vaporization of Al under vacuum during the EB-PBF process. Al-, or Fe-riched particles observed in the reused powder may contribute to fluctuation once a few of these contaminants exist in the tested powder samples.

Therefore, the results from the bulk EB-PBF-built samples should be more trustable.

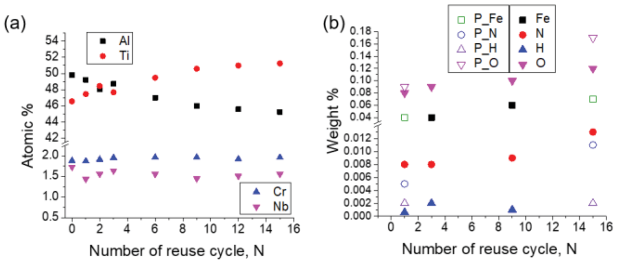

Fig. 3. (a) Ti, Al, Nb, Cr changes with the reuse cycles, measured from powder by using EDS method. (b) Chemical compositions change of the trace elements under the different number of recycling by ICP, measured both from EB-PBF parts and powder. P_ indicated the measurements from powder.

On the other hand, we observed a consistent increase of Fe in both powder and EB-PBF-built samples. The increase in Fe contaminant present in the powder sample could be due to the metallization of the heat shields and the contaminants falling onto the powder bed during the EB-PBF process and cooling down stage after the EB-PBF process. Other sources may relate the wear debris from the rake blades, rake arm, flaps and PRS. This can be further confirmed by the change of Fe content in the EB-PBF-built TiAl, where the Fe increased from 0.04% to 0.07%. Fig. 4 shows some film-like Fe-riched contaminants that either embedded into the deformed powder surface or attached to the undeformed powder surface.

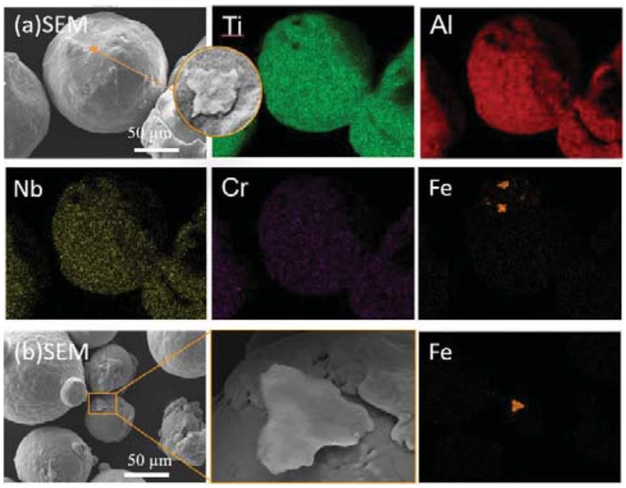

Fig. 4. Film-like contaminants (a) embedded into the Ti-48Al-2Cr-2Nb powder and (b) attached on the Ti-48Al-2Cr-2Nb powder.

Substantial oxygen and nitrogen pick-up is also observed as the powder is being reused due to blasting in the PRS, speeding up the oxidation process by generating new oxidation-prone surfaces on the powder particles [11]. In addition, the sieving and shifting of the powder are under an ambient atmosphere, which is considered another factor leading to the abnormally rapid increase in the oxygen and nitrogen level of the powder [11]. The main component of the surface oxide film is confirmed to be TiO_2/Ti_2O_3 and Al_2O_3 because of the sharp increase in Ti and Al concentrations at the first nanometers by XPS analysis. The first XPS profiles of the R0 and R15 powders contained peaks that corresponded to the major alloying elements (Ti 2p, Al 2p, Cr 2p, Nb 3d), besides carbon (C 1s) and very strong oxygen (O 1s) peaks. No differences in the peak positions indicated that the chemical compositions and types of compounds on the surface of the powders were consistent.

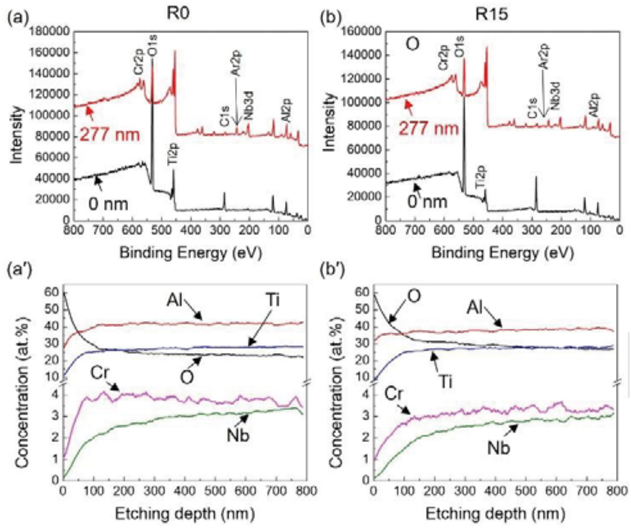

Fig. 5. X-ray photoelectron spectroscopy (XPS) survey spectra of Ti-48Al-2Cr-2Nb powders: (a) Virgin powder; (b) R15 powder. The atomic concentration of O, Al, Ti, Cr, and Nb against sputtering depth (nm) for (a′) virgin power, (b″) reused cycle 15 powder.

To investigate the effect of recycling powders on the surface oxide layer, XPS depth profiling was conducted on virgin (R0) and reused (R15) Ti-48Al-2Cr-2Nb powders. The atomic concentrations against sputtering depth for respective samples are shown in Fig. 5 (a′ and b′). The oxygen content decreased while the other elements climbed as the sputtering time increased. This indicates the presence of oxides on the surface of the powders and the oxides only appear in the outermost layer and in film form. Here we considered a sputtering depth when the oxygen concentration reaches its half-maximum as the oxide-substrate interface. The estimated oxide thicknesses were 31 nm and 43 nm for R0 and R15 powders, respectively. Although the thickness increment is not very significant, there are more Ti-oxides on the surface and the surface oxide structure may be more stable.

However, it is interesting to note that oxygen content reduces significantly in the EB-PBF-built Ti-48Al-2Cr-2Nb when compared with the powder, especially in the 15^{th} cycle, as shown in Fig. 3 (b). The oxygen reduced from 0.17% (powder) to 0.12% (EB-PBF-built part), indicating that the vacuum of the EB-PBF process can be used as purification. It is hypothesized that these oxides may dissociate in the molten pool. Fig. 6 shows the equilibrium oxygen partial pressures of selected oxides as a function of temperature. The dashed line in Fig. 6 indicated the oxygen partial pressure (2.59×10^{-9} bar) during the EB-PBF process monitored with a residual gas analyzer by Terrazas *et al.* [14]. This value is lower than the oxygen dissociation partial pressures of metal oxides like Al_2O_3, TiO_2, Ti_2O_3, Cr_2O_3, Nb_2O_5 at a temperature of about 1775 ℃, 1500 ℃, 2000 ℃, 1388 ℃, 1400 ℃, respectively. It is reported that the molten pool temperature in the EB-PBF process can reach up to more than 3000℃ [15]. The green zone indicated the temperature range in the molten pool. Above each of their critical temperature, these metal oxides dissociate in the molten pool and the oxygen is released from the molten pool. The release of oxygen from the molten pool reduces the oxygen concentration in the EBM-built Ti-48Al-2Cr-2Nb, acting as a refining process.

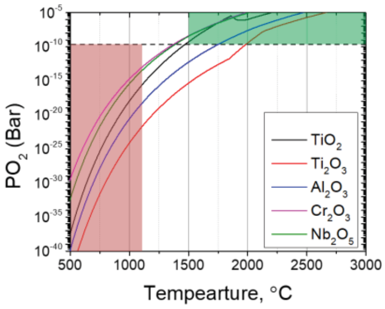

Fig. 6. Equilibrium oxygen partial pressures of selected oxides as a function of temperature.

Fig. 7 shows the microstructure of B3 and B15 of EB-PBF-built Ti-48Al-2Cr-2Nb. There is no apparent grain preference. The dominant phase for both samples is the γ phase, which reached more than 98%, in agreement with the previous reports [16, 17]. However, the grain size of the γ phase decreased from 14.9 μm to 10.8 μm. In addition, the α_2 (Ti_3Al) phase increases from 1.28% to 1.57% due to the reduction of Al content during the powder reuse. It is reported that the Ti3Al phase increase with the loss of Al contents in Ti-Al intermetallic [18]. The compression stress-strain curve under different reuse times did not show a visible difference from B1 to B15. The compressive YS for B1, B9 and B15 were 586±5 MPa, 596±8 MPa, and 593±8 MPa. Therefore, we can conclude that powder reuse did not change the compressive property within the 15 cycles.

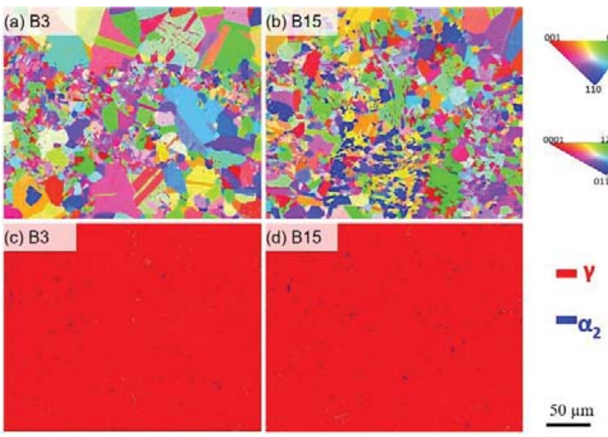

Fig. 7 Microstructure in the B3 and B15 of EB-PBF-built Ti-48Al-2Cr-2Nb.

4. Conclusions

The particle size distribution became narrow by removing both the fine particles and coarsen particles during the reuse cycle. The apparent density and tapped density increase with the number of reuse cycles. Flowability became better with the increase in reuse cycles. Powder morphology changed with the number of recycling cycles. Removing the fine particles, destroying the spherical particle, and adding the irregular contaminants were observed with the reuse cycles. No visible change in resultant microstructure and the mechanical property was observed, although the chemical composition changed with the reuse cycles. This means the same batch of powder can be reused up to 15 times without compromising the performance of their final parts.

ACKNOWLEDGEMENT

The Hitachi-SIMTech joint lab financially supported the work in the research. The authors thank Dr. Guixuan Wu from GTT-Technologies (Germany) for support in thermodynamics calculation with FactSage and an intern from SIMTech, Mr. Nicholas Tan for support in the sample preparation.

REFERENCES

1. Juechter, V., M.M. Franke, T. Merenda, A. Stich, C. Koerner, R.F. Singer, "Additive manufacturing of Ti-45Al-4Nb-C by selective electron beam melting for automotive applications", Addi. Manuf., Vol.22, pp. 118-126, 2018.
2. Wang, P., X. Li, S. Luo, M.L.S. Nai, J. Ding, J. Wei, "Additively manufactured heterogeneously porous metallic bone with biostructural functions and bone-like mechanical properties", J. Mater. Sci. Technol., Vol.62, pp. 173-179, 2021.
3. Baudana, G., S. Biamino, B. Klöden, A. Kirchner, T. Weißgärber, B. Kieback, M. Pavese, D. Ugues, P. Fino, C. Badini, "Electron Beam Melting of Ti-48Al-2Nb-0.7Cr-0.3Si: Feasibility investigation", Intermetallics, Vol.73, pp. 43-49, 2016.
4. Tang, H.P., G.Y. Yang, W.P. Jia, W.W. He, S.L. Lu, M. Qian, "Additive manufacturing of a high niobium-containing titanium aluminide alloy by selective electron beam melting", Mater. Sci. Eng., A, Vol.636, pp. 103-107, 2015.
5. Yue, H., H. Peng, R. Li, J. Yang, R. Gao, S. Zhang, X. Wang, Y. Chen, "Metastable phase and microstructural degradation of a TiAl alloy produced via selective electron beam melting", Vacuum, Vol.192, pp. 110491, 2021.
6. Ge, W., C. Guo, F. Lin, "Effect of Process Parameters on Microstructure of TiAl Alloy Produced by Electron Beam Selective Melting", Procedia Eng., Vol.81, pp. 1192-1197, 2014.
7. Chen, W., Z. Li, "Additive manufacturing of titanium aluminides", pp. 235-263, 2019.
8. Davies, S., GE Aviation GE9X engine receives FAA certification, 2020. (Accessed 2022.01.12.
9. Wang, P., P. Huang, F.L. Ng, W.J. Sin, S. Lu, M.L.S. Nai, Z. Dong, J. Wei, "Additively manufactured CoCrFeNiMn high-entropy alloy via pre-alloyed powder", Mater. Des., Vol.168, pp. 107576, 2019.
10. Bale, C.W., E. Bélisle, P. Chartrand, S.A. Decterov, G. Eriksson, A.E. Gheribi, K. Hack, I.H. Jung, Y.B. Kang, J. Melançon, A.D. Pelton, S. Petersen, C. Robelin, J. Sangster, P. Spencer, M.A. Van Ende, "Reprint of: FactSage thermochemical software and databases, 2010–2016", Calphad, Vol.55, pp. 1-19, 2016.
11. Moghimian, P., T. Poirié, M. Habibnejad-Korayem, J.A. Zavala, J. Kroeger, F. Marion, F. Larouche, "Metal powders in additive manufacturing: A review on reusability and recyclability of

common titanium, nickel and aluminum alloys”, Addi. Manuf., Vol.43, pp. 102017, 2021.

12. Powell, D., A.E.W. Rennie, L. Geekie, N. Burns, “Understanding powder degradation in metal additive manufacturing to allow the upcycling of recycled powders”, J. Clean Prod., Vol.268, pp. 122077, 2020.
13. Tang, H.P., M. Qian, N. Liu, X.Z. Zhang, G.Y. Yang, J. Wang, “Effect of Powder Reuse Times on Additive Manufacturing of Ti-6Al-4V by Selective Electron Beam Melting”, JOM, Vol.67, No.3, pp. 555-563, 2015.
14. Terrazas, C.A., J. Mireles, S.M. Gaytan, P.A. Morton, A. Hinojos, P. Frigola, R.B. Wicker, “Fabrication and characterization of high-purity niobium using electron beam melting additive manufacturing technology”, Int. J. Adv. Manuf. Technol., Vol.84, , pp. 1115-1126, 2016.
15. Zhao, Y., K. Aoyagi, K. Yamanaka, A. Chiba, “Role of operating and environmental conditions in determining molten pool dynamics during electron beam melting and selective laser melting”, Addi. Manuf., Vol.36, pp. 101559, 2020.
16. Kim, Y.-K., S.-J. Youn, S.-W. Kim, J. Hong, K.-A. Lee, “High-temperature creep behavior of gamma Ti-48Al-2Cr-2Nb alloy additively manufactured by electron beam melting”, Mater. Sci. Eng., A, Vol.763, pp. 138138, 2019.
17. Seifi, M., A.A. Salem, D.P. Satko, U. Ackelid, S.L. Semiatin, J.J. Lewandowski, “Effects of HIP on microstructural heterogeneity, defect distribution and mechanical properties of additively manufactured EBM Ti-48Al-2Cr-2Nb”, J. Alloys Compd., Vol.729, pp. 1118-1135, 2017.
18. Gasper, A.N.D., S. Catchpole-Smith, A.T. Clare, “In-situ synthesis of titanium aluminides by direct metal deposition”, J. Mater. Process. Technol., Vol.239, pp. 230-239, 2017.